High-pressure melting curve of sulfur up to 65 GPa

Sarah M. Arveson, Yue Meng, June Lee, and Kanani K. M. Lee

Phys. Rev. B **100**, 054106 — Published 15 August 2019

DOI: 10.1103/PhysRevB.100.054106

The High-Pressure Melting Curve of Sulfur to 65 GPa

Sarah M. Arveson

Department of Geology & Geophysics,

Yale University, New Haven CT 06511

Yue Meng

HPCAT, X-Ray Science Division, Argonne National Laboratory, Argonne, IL 60439

June Lee

American School of Dubai, Dubai, United Arab Emirates

Kanani K. M. Lee

Department of Geology & Geophysics,

Yale University, New Haven CT 06511

(Dated: July 23, 2019)

Abstract

The melting curve of elemental sulfur was measured to pressures of 65 GPa in a laser-heated diamond-anvil cell using ex-situ textural analyses combined with spectroradiometry and benchmarked with laser-power-temperature functions. The melting curve reaches temperatures of ∼1800 K by 65 GPa and is smooth in the range of 23-65 GPa with a Clapeyron slope of ∼14 K/GPa at 23 GPa. This is consistent with melting of a single tetragonal sulfur structure in this range, which is confirmed by in-situ x-ray diffraction. An updated equation of state for tetragonal sulfur is determined, and the high-pressure, high-temperature stability region of tetragonal sulfur is reassessed.

I. INTRODUCTION

Sulfur is the tenth most abundant element in the universe and the fifth most abundant element on Earth. It plays a major role in planetary volcanism and is thought to be present in many planetary cores due to its presence in iron meteorites[1]. Despite the ubiquity of sulfur, the high-pressure melting curve of elemental sulfur has not been measured beyond 12.5 GPa[2,3], and the nature of sulfur at high pressures and temperatures remains largely either contested or uncharacterized. Elemental sulfur undergoes a number of complex structural phase transitions at high pressures, including amorphization and metallization, though few studies agree on exactly what these crystal structures are or where the phase boundaries occur[4–9]. Sulfur has attracted attention for its wide range of allotropes, adopting ring structures ranging from S_6 to S_{20}, chain structures, and helices depending on synthesis conditions and thermodynamic conditions in the bulk phase[10]. Conducting monatomic chains have also been observed for 1D sulfur confined by carbon nanotubes[11]. At high pressures and temperatures, it has been shown that sulfur alternates between different allotropes, adopting an S_8 ring structure in the orthorhombic phase[12], a triangular chain structure in the trigonal phase[9,13], an S_6 ring structure in the rhombohedral phase[9], and a square chain structure in the tetragonal phase[13]. At atmospheric pressure and temperatures near the melting point, the melt is yellow and has a short-range structure similar to that of the solid with S_8 rings, but at higher temperatures, transforms to a higher viscosity red liquid with a different polymerization state[14]. Liquid-liquid transitions in sulfur have been observed at high pressure and correlated to these changes in sulfur allotropes[3] or chain breakage[15], so changes in the shape of the melting curve at higher pressures may signify liquid-liquid transitions related to short-range structural changes in molten sulfur.

Early studies determined melting of sulfur up to 6 GPa by differential thermal conductivity analysis, using a discontinuity in thermal conductivity to infer melting[16,17]. Other Group VI elements like Se and Te exhibit a concave melting curve below 4.5 GPa[16]. For sulfur, some studies prescribe linearly increasing melting in this pressure range with a slope of 300 K/GPa[17], while others find multiple changes in concavity in this range[18]. A later study used electrical measurements and thermobaric methods to investigate the melting curve and melt structure between 5.5 GPa and 12.5 GPa[2,3]. The authors inferred two liquid-liquid transitions, the latter being due to metallization of the sulfur melt near 12 GPa, a much

lower pressure than the solid insulator-to-metal transition[19], and corresponding to a volume decrease in the melt.

More recently, strides have been made in the accuracy of pressure and temperature calibration at high pressures, warranting further exploration of sulfur melting at pressure. Developments in continuous wave (CW) laser heating during in-situ high-pressure, high-temperature (HPHT) synchrotron x-ray diffraction (XRD) allow for precise alignment of XRD sampling region with respect to the heated region as well as rapid measurement of temperature and XRD during heating[20]. Two-dimensional temperature mapping in conjunction with electron microscopy provides a new, independent method for determining melting temperatures at high pressures[21], and correct temperature measurements can be made by taking into account wavelength-dependent absorption of materials in the sample chamber[22]. Phase transitions in solid sulfur at higher pressures as well as evolution towards the metallic state will likely affect the nature of the melting curve at higher pressures. While data for the high-pressure, room temperature solid phases of sulfur extends to several hundred GPa[5–8,12], the HPHT solid phase diagram of sulfur is largely unknown. We performed laser-heated diamond anvil cell (LHDAC) experiments to characterize the melting curve of sulfur, using quenched textures to determine the melting temperature. We also used in-situ HPHT synchrotron XRD to probe the crystal structure prior to melting.

II. METHODS

Sulfur powder (Alfa Aesar, 99.5% purity) was pressed into a disk, ∼100 μm in diameter and 10 – 20 μm-thick, and loaded into the sample chamber of a pre-indented rhenium gasket in a diamond-anvil cell. Either KBr, KCl, or Ne was used as an insulation medium and pressure-transmitting medium. Stepped anvils were used to make even layers of insulation to ensure steady heating[23]. The starting material was confirmed via powder x-ray diffraction as orthorhombic sulfur with space group *Fddd*, the expected phase at ambient conditions[24]. Scanning electron microscope (SEM) images confirmed that the starting grain size prior to heating varied between ∼0.1 and 1 μm. Samples were compressed to a pressure between 26 – 65 GPa using diamond anvils with a culet size of either 200 or 300 μm. Pressure was measured before and after heating using the Raman shift of the diamond edge[25] or, when available, the room-temperature equation of state of KCl[26] or Ne[27]. We did not take into

account thermal pressure.

To melt sulfur at high pressures, we performed two types of LHDAC experiments. The first set of experiments were performed in the Yale University Department of Geology & Geophysics using multi-wavelength imaging radiometry (i.e., four-color method) and electron microscopy[21,28]. For the first set of experiments, sulfur was heated at pressures up to 65 GPa using a 1070 nm fiber CW laser[21]. The samples were subjected to either single-sided steady heating at a constant power or single-sided predefined ramp heating, in which the sample is annealed at a low laser power, ramped to a peak power, and held at the peak power until the laser was shut off[28]. As sulfur melting temperatures are relatively low, samples were heated at their peak power for a duration between 20 seconds and 2 minutes in order to have enough thermal radiation to accurately measure temperatures. When the sample reached its maximum temperature, the intensity of emitted light from the sample was collected onto a CCD simultaneously at four wavelengths (580 nm, 640 nm, 766 nm, and 905 nm) across the heated region, typically between 20 – 50 μm in diameter. The spectrum was then fit to a Wien function to extract a temperature in each pixel, producing a 2D temperature map of the hotspot. Because the thermal emission was magnified onto the CCD, the spatial resolution of each CCD pixel was 0.48 μm $\times$ 0.48 μm. Error sources from averaging and fitting led to a 5 – 6% error in temperature measurement. Further details on temperature measurement setup and accuracy can be found in Ref.[21].

To complement these results, we also performed in-situ HPHT synchrotron XRD[20] experiments of sulfur, up to 53 GPa at room temperature and at high temperatures for experiments at $\sim$23 GPa and $\sim$44 GPa, at Sector 16-ID-B of the Advanced Photon Source at Argonne National Lab using an x-ray wavelength 0.4066 $\mathring{A}$. The samples were subjected to double-sided heating, and temperatures were determined by fitting the Planck radiation function to the measured blackbody radiation between 600 – 800 nm from a spatially selected area 4 μm in diameter on the heated sample[20]. We gradually increased the heating laser power and at each stepwise increase of laser power, temperature measurements and diffraction patterns were taken with 20-second exposures. Samples were heated continuously for up to 1 hour.

To confirm that sulfur does not have wavelength dependent absorption that can affect temperature measurement, we performed hgh-pressure optical absorption measurements between 400 and 1050 nm at the Infrared Lab of the National Synchrotron Light Source II at Brookhaven National Laboratory. The visible absorption spectra were collected through a

customized visible microscope system together with a spectrograph (SpectraPro SP-2556, Princeton Instruments) and a liquid nitrogen cooled PyLoN CCD detector. A reference spectrum was taken through an adjustable iris aperture at a transparent KCl area at each pressure. We limited the lowest pressures of our study to ∼23 GPa, above which sulfur is optically opaque (Fig. S1). At low pressures[14,29,30] and between ∼12 – 25 GPa, sulfur has highly wavelength-dependent absorption in the visible spectrum (Fig. S1) so that temperatures are aliased unless a full set of in-situ HPHT visible absorption measurements are made, and a temperature correction is applied[22]. Under the experimental conditions of our study, sulfur has a wavelength-independent absorption profile between 600 – 800 nm, wherein our thermal emission data is collected. Since a wavelength independence in absorption functionally implies a wavelength independence in emissivity, we assumed graybody radiation.

III. RESULTS

A. Identification of melt

Our primary method for identifying melt is analysis of quenched texture. This method has been benchmarked against others and shown to be reliable for a variety of metals[21,31] and oxides[28]. Prior to melting, the hotspot is nearly indistinguishable from the unheated material (Fig. 1A). Melted hotspots show a distinct, round and raised bleb of sulfur (Fig. 1B – 1D). The boundary of this bleb forms an isotherm where solid and liquid coexist. We integrated the temperatures along this boundary using a 2D temperature map to find a single melting temperature with a typical standard deviation of 20 K or less over hundreds of pixels which is included in the total systematic measurement error of 5 – 6%.

Melt blebs are raised with respect to the surface of the original unheated sample (Fig. S2). Nearly all of our quenched melt blebs show holes where molten sulfur rose up into the insulation medium (Fig. 2) similar to the inference of Al_2O_3 chunks falling into molten metal in Ref.[32]. Because all pore space must be closed at high pressures, the holes observed in the quenched melt blebs must have been filled while melted in-situ. We infer that the holes were filled with solid insulation medium (KBr or KCl) when the sulfur melted. When the salts were dissolved from the sample using H_2O after quenching, the holes persisted,

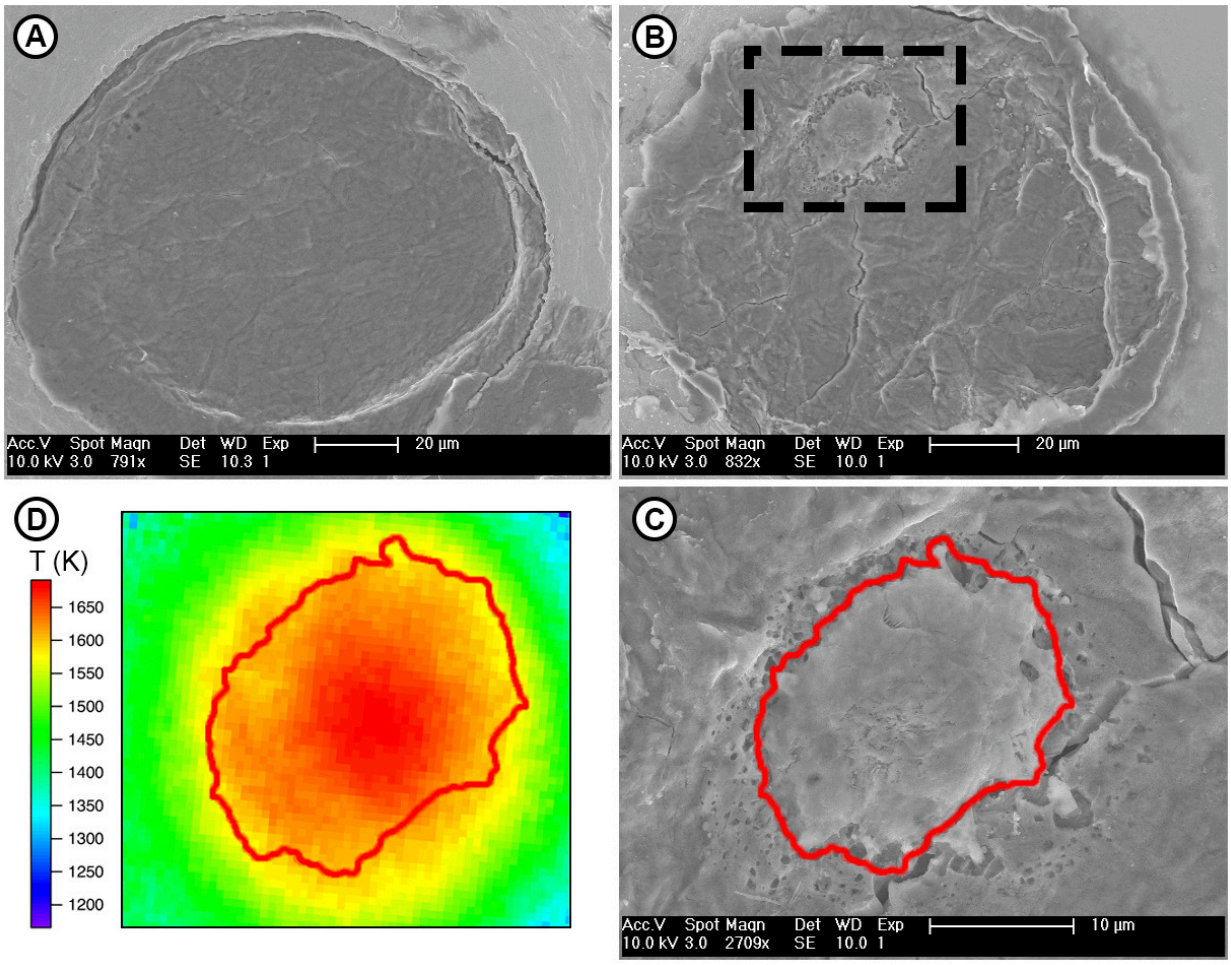

FIG. 1. Mapping melt texture to 2D temperature maps. **(A)** A sample heated to a peak temperature of 1370 K at 51 GPa showing no melt bleb. **(B)** A sample heated to a peak temperature of 1680 K at 51 GPa showing a distinct melt bleb. **(C)** Zoom in of dotted region in (B) of a sulfur melt bleb and its boundary. **(D)** Melt boundary superimposed on the temperature map which is integrated to determine a melting temperature of 1600 (± 100) K.

allowing their observation with electron microscopy (Fig. 2).

We also use plateaus in the laser power-temperature function as an additional check for melting. The method of using plateaus in temperature versus laser power has been commonly used for identifying melting at high pressures in LHDAC[33,34] and multi-anvil[35] experimental setups. The plateaus are ascribed to a release of latent heat during the melting transition, but it has been shown that unrelated changes in sample reflectivity or thermal conductivity can also cause apparent plateaus[36]. The plateaus observed during our laser

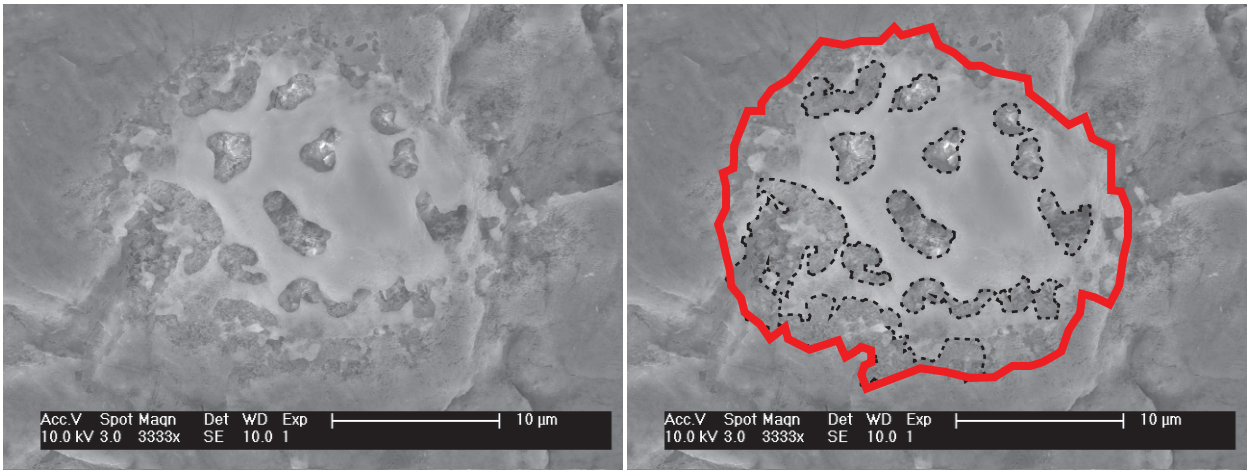

FIG. 2. SEM image of a melt spot on a sample heated at 34 GPa to a peak temperature of 1630 K showing holes where KBr fell into the melt and was dissolved with water after quenching. The melt boundary is outlined in red, and the holes are outlined in black dashes.

heating experiments with in-situ XRD agree with temperatures derived from our texture and temperature mapping technique (Fig. 3, 4). In our diffraction experiments, we observe the temperature continue to plateau with increasing laser power. This is consistent with observation during textural analysis, namely, increasing the laser power increases the surface area of the melt, rather than significantly raising the temperature of the liquid sulfur above its melting temperature (Fig. S3, S4).

We were not able to detect diffuse scattering in the diffraction patterns. The conditions for observing diffuse scattering for a low-Z material such as sulfur are specific and difficult to tune. One major setback is the small vertical (on-heating-axis) extent of melt produced in these experiments. Our quenched melt blebs are typically $\sim$20 – 50 μm in diameter. The x-ray spot (nominally $\sim$4 μm $\times$ 5 μm and orthogonal to the melt bleb) thus only probes a small portion of this. Assuming 1 – 2 μm melt depth for a 20 μm-thick sample (Fig. S2), this is only $\sim$5 – 10% of the volume of the sulfur probed, which is then further obscured by diffraction signal from the crystalline insulation media. Additionally, we find that texturally, as we increase laser power, the temperature does not go up (i.e., the laser power-temperature plateau), but the lateral extent of the melt bleb increases (Fig. S3, S4). This suggests that the temperature along the heating axis does not increase significantly, and the extra energy instead partitions into increasing the size of melt bleb in the direction of least temperature gradient.

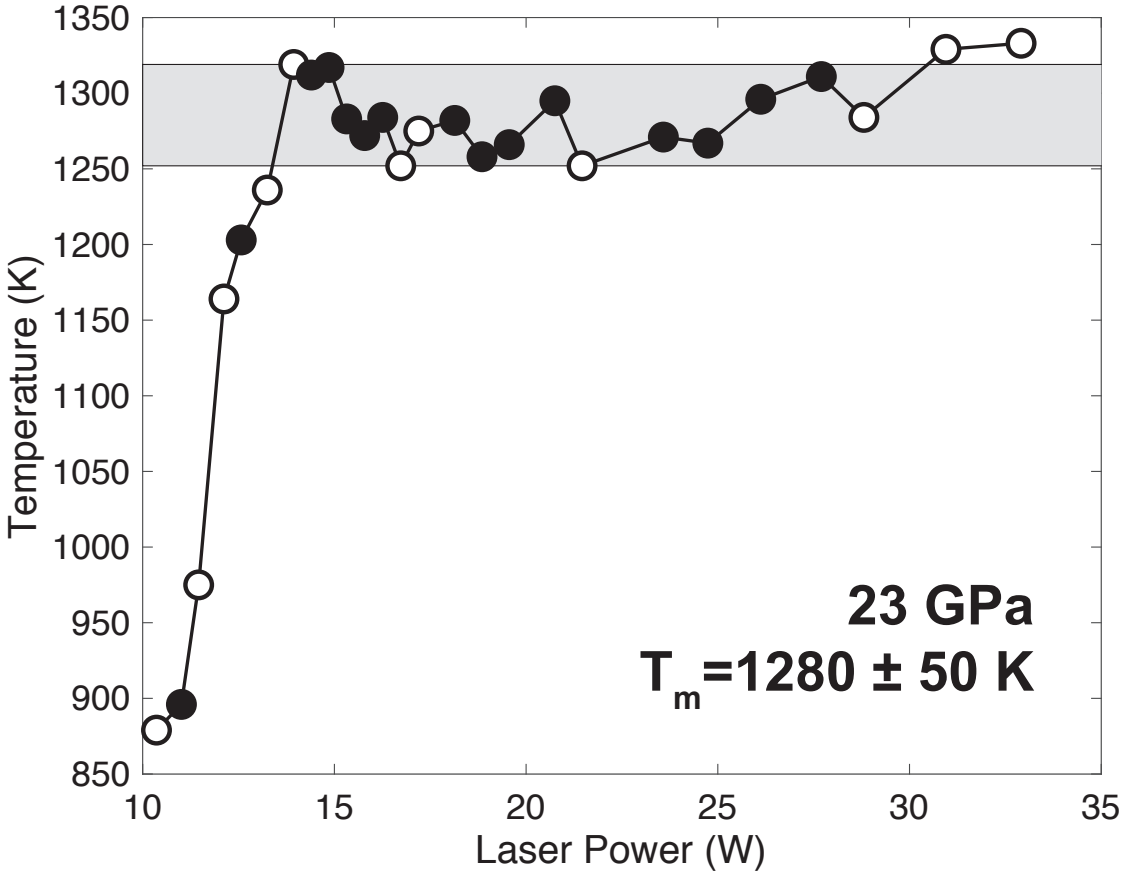

FIG. 3. Laser power-temperature relationships during heating of a sulfur sample at 23 GPa using KCl as thermal insulation. Samples were heated from both sides using a CW infrared laser and slowly ramping up the power. Temperatures are determined by fitting Planck radiation the black-body radiation at 600 nm – 800 nm from a spatially selected area ~ 4 μm in diameter on the heated sample[20]. Temperature increases rapidly and nearly linearly below the melting point. Once the melting point is reached, the temperature fluctuates around a plateau (grey shaded region) before the temperature begins to increase again. The entire heating duration was 26 minutes. Open symbols are those for which raw diffraction patterns are shown in Fig. S7.

B. High-pressure melting curve

The melting curve between 26 GPa and 65 GPa has a Clapeyron slope of 14 K/GPa at our reference pressure of 23 GPa for a Simon-Glatzel-type fit to our melting curve (Fig. 4). A Simons-Glatzel-type fit to the textural data yields $T_m = T_{m,ref}(\frac{P-P_{ref}}{a} + 1)^{\frac{1}{c}}$ with a =

64.84 GPa and c = 1.41 for temperatures measured in kelvin.

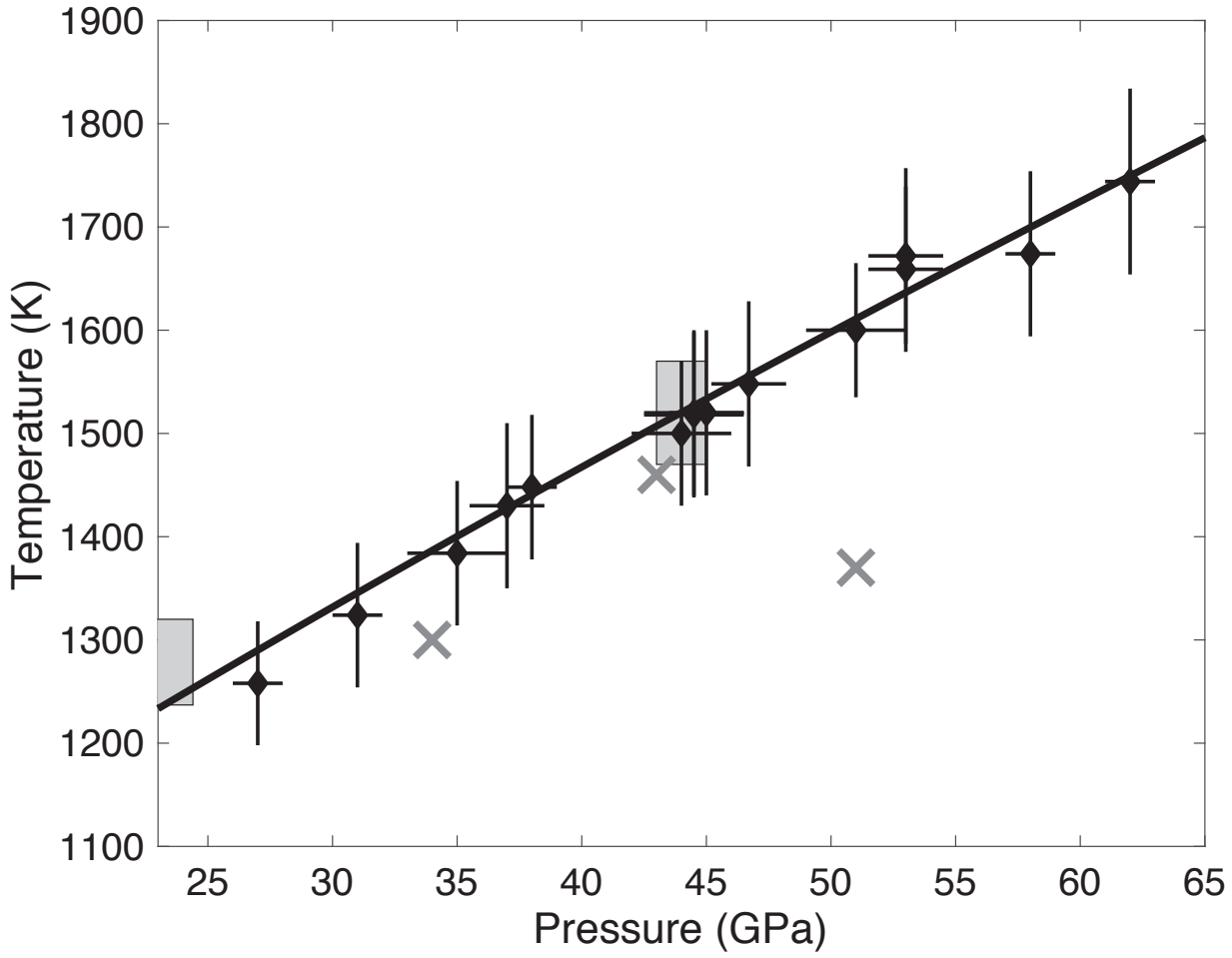

FIG. 4. The extended high-pressure melting curve of sulfur. Diamonds are melting points from textural mapping, and grey shaded bars are laser power-temperature inferred melting temperatures. "X" symbols are samples heated to temperatures which did not show any textural evidence of melting. The curve is a Simons-Glatzel fit to the textural data $T_m = T_{m,ref}(\frac{P-P_{ref}}{a} + 1)^{\frac{1}{c}}$ with a=64.84 and c=1.41.

An extrapolation of our melting curve to lower pressures agrees well with the previous dataset that represented the highest pressure melting curve of sulfur to 12.5 GPa[2]. The fit is only to the textural melting data, but the melting temperatures inferred from laser power-temperature plateaus fall remarkably well on the curve, suggesting that this may be a viable method for extending the melting temperature to even higher pressures. Once the temperature reaches a plateau at the melting temperature, it becomes exceedingly difficult to heat the sample well above its melting temperature. This is consistent with behavior we

observe during melting with the four-color method as well – with increasing laser power, the temperature of the sample increases very little with increasing laser power once the melting temperature is reached, suggesting a significant change in thermal properties upon melting or thereafter. While no previous studies have examined thermal properties of sulfur at high pressures across the high-pressure melting transition to which we can assign this material property change, a jump in electrical conductivity and hence thermal conductivity has been observed across the L'- L" liquid-liquid transition[2]. Existing melting curves of sulfur disagree by up to ∼250 K at 3 GPa[8,9,16,37]. While LHDAC experiments cannot reconcile such low pressure data due to diamond metastability, they extend the melting curve to much higher pressures and offer clues into the largely unknown polymorphism of sulfur at HPHT conditions.

C. High-(P, T) solid phases

Using no pressure medium, two previous studies[5,12] observed the tetragonal phase appear at 54.5 GPa after inferring amorphous sulfur persisting from 23 GPa. Here, neon is used in an experiment to monitor the room temperature compression sequence under quasi-hydrostatic conditions. We observed the transition to tetragonal sulfur at room temperature at 38 GPa, similar to the pressures reported in experiments that used N_2 (36 GPa)[8] and He (37.5 GPa)[7] as pressure media. The discrepant transition pressures between this study and the others[7,8] may originate from different methods of pressure calibration and varying degrees of non-hydrostaticity. We do not observe amorphization but do note significant peak broadening between 36 GPa and 38 GPa before the sharp tetragonal transition indicative of slow kinetics (Fig. S5).

The tetragonal sulfur observed is consistent with the $I4_1/acd$ space group assignment[7]. This phase of sulfur has been called S-II and S-III in the literature, but we refer to it here as simply "tetragonal sulfur" to avoid confusion caused by discrepant nomenclature. We observe tetragonal sulfur persisting at room temperature from 38 GPa to at least 54 GPa (Fig. S6), the highest pressure probed in our XRD experiments. The structure quenches on decompression to at least 19 GPa (the lowest pressure to which we decompressed), consistent with a previous observation that tetragonal sulfur remains metastable on decompression to at least 3 GPa[13]. Using a third-order Birch-Murnaghan formulation, the room-temperature

equation of state (EOS) with K_0' fixed to 4.5, we find $V_0 = 21.9 \pm 1$ $\mathring{A}^3$ and $K_0 = 23.7 \pm 1$ GPa. Previous data[7,8] fall well on our independent EOS extrapolated at lower pressures to 5 GPa and higher pressures to 90 GPa (Fig. 5, Table S1).

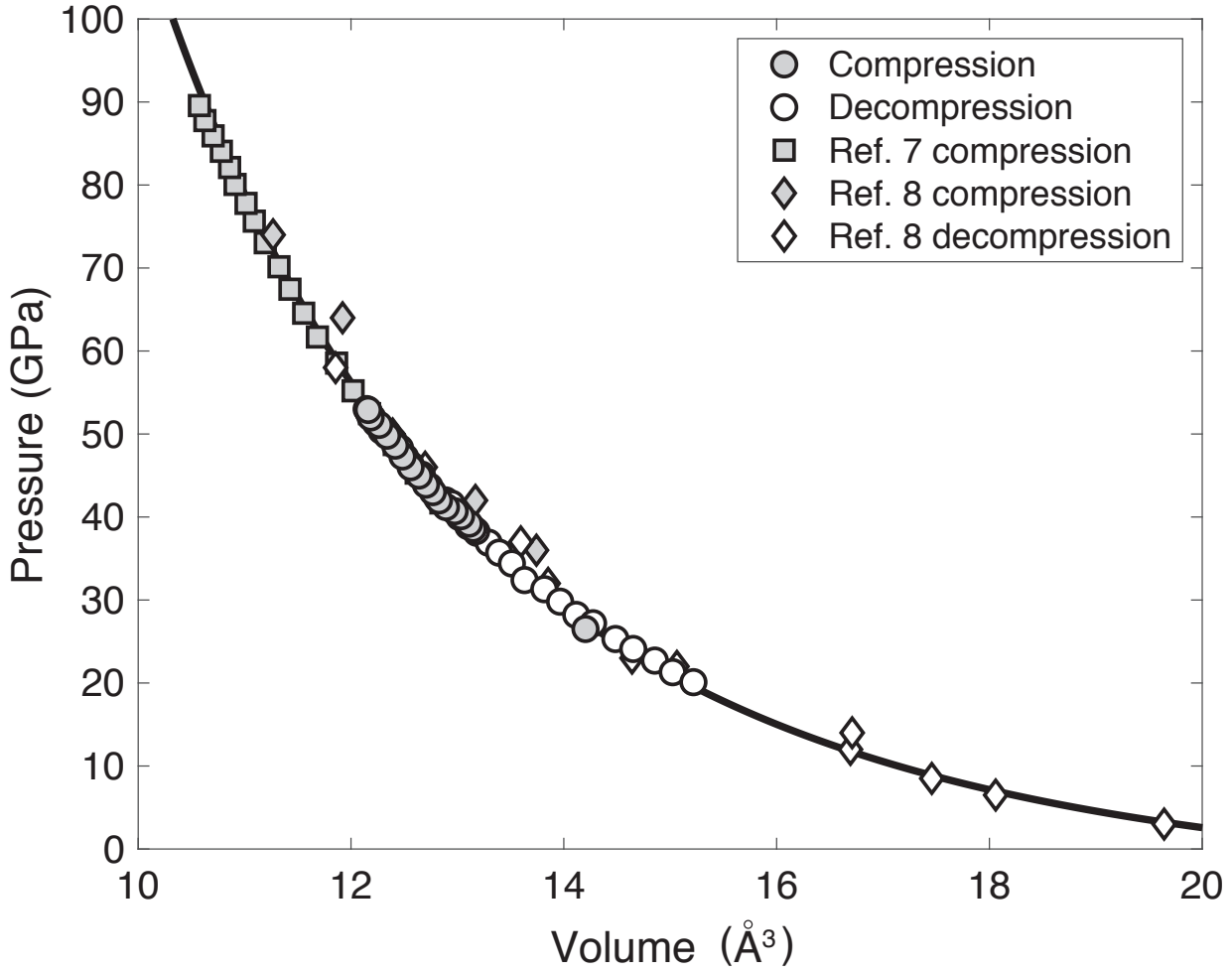

FIG. 5. Room-temperature tetragonal sulfur volumes as a function of pressure. Filled (open) symbols are shown for volumes collected on compression (decompression) for this study (circles), Ref.[8] (squares) and Ref.[7] (diamonds). A third-order Birch-Murnaghan equation of state fit to only our data is shown as a black curve. Extrapolation to higher and lower pressures agree remarkably well with existing data in Ref.[7,8].

In two heating runs, we observed that the tetragonal structure is stable upon heating (Fig. 6) and that sulfur melts in the tetragonal structure. At 23 GPa, the sulfur transforms into the tetragonal structure between 300 K and 896 K, the first temperature upon heating that was resolvable, and remains in said structure until it melts at ∼1280 K. At 44 GPa,

the tetragonal structure persists from 300 K to the melting point at ∼1530 K. Examples of in-situ heating patterns can be found in Fig. 7 with corresponding data in Table S2. These heating runs extend the currently known stability range of tetragonal sulfur to higher pressures and temperatures (Fig. 8).

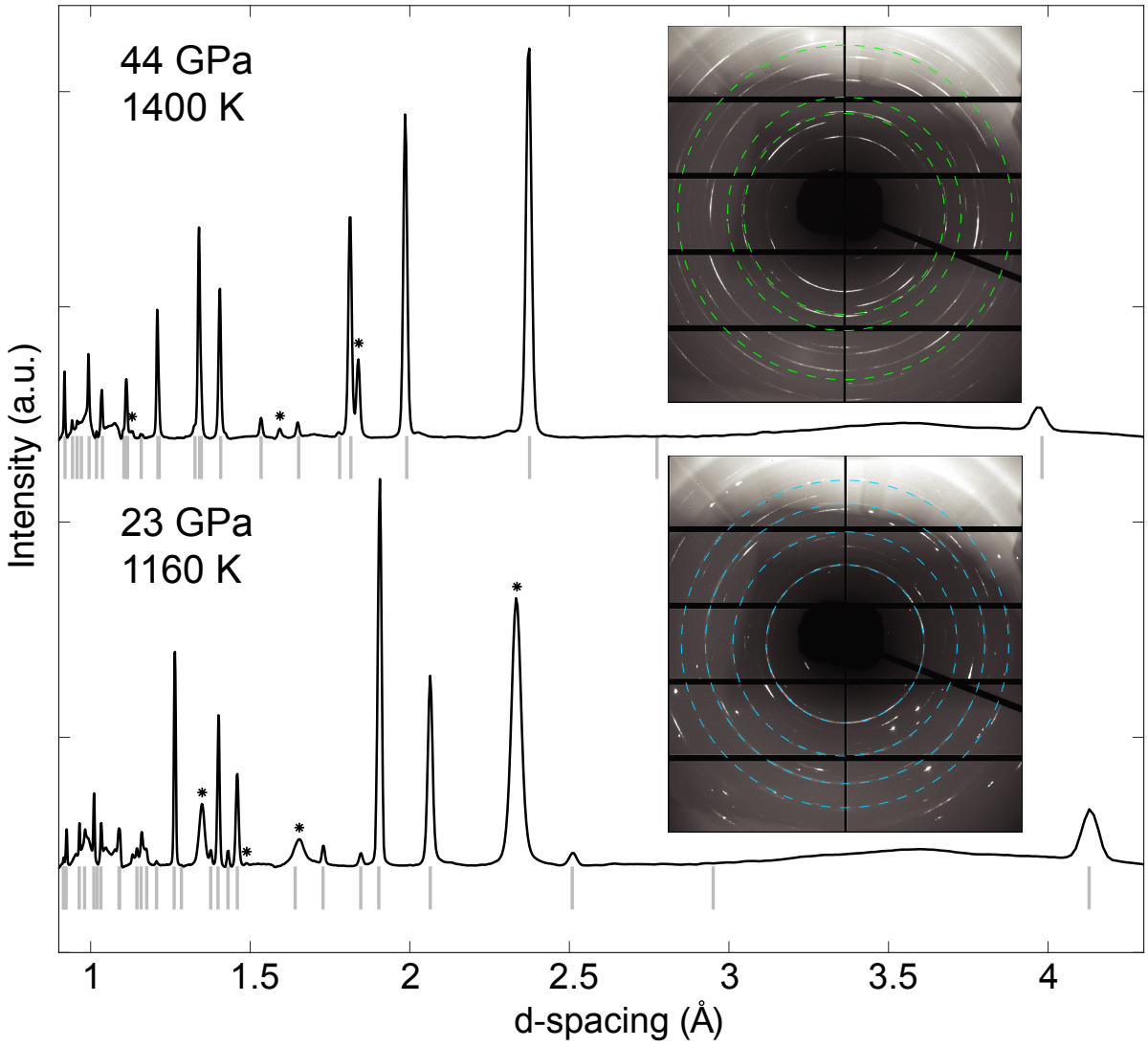

FIG. 6. Examples of integrated tetragonal sulfur diffraction patterns at high temperatures with corresponding raw images shown inset. Grey ticks mark the fitted peaks for sulfur in the $I4_1/acd$ structure (16 atoms per unit cell). Asterisks (integrated patterns) and dashed circles (raw images) denote diffraction from the insulation/pressure media (Ne at 44 GPa, KCl at 23 GPa). Pressures are derived from the pressure medium and neglect the effect of thermal pressure.

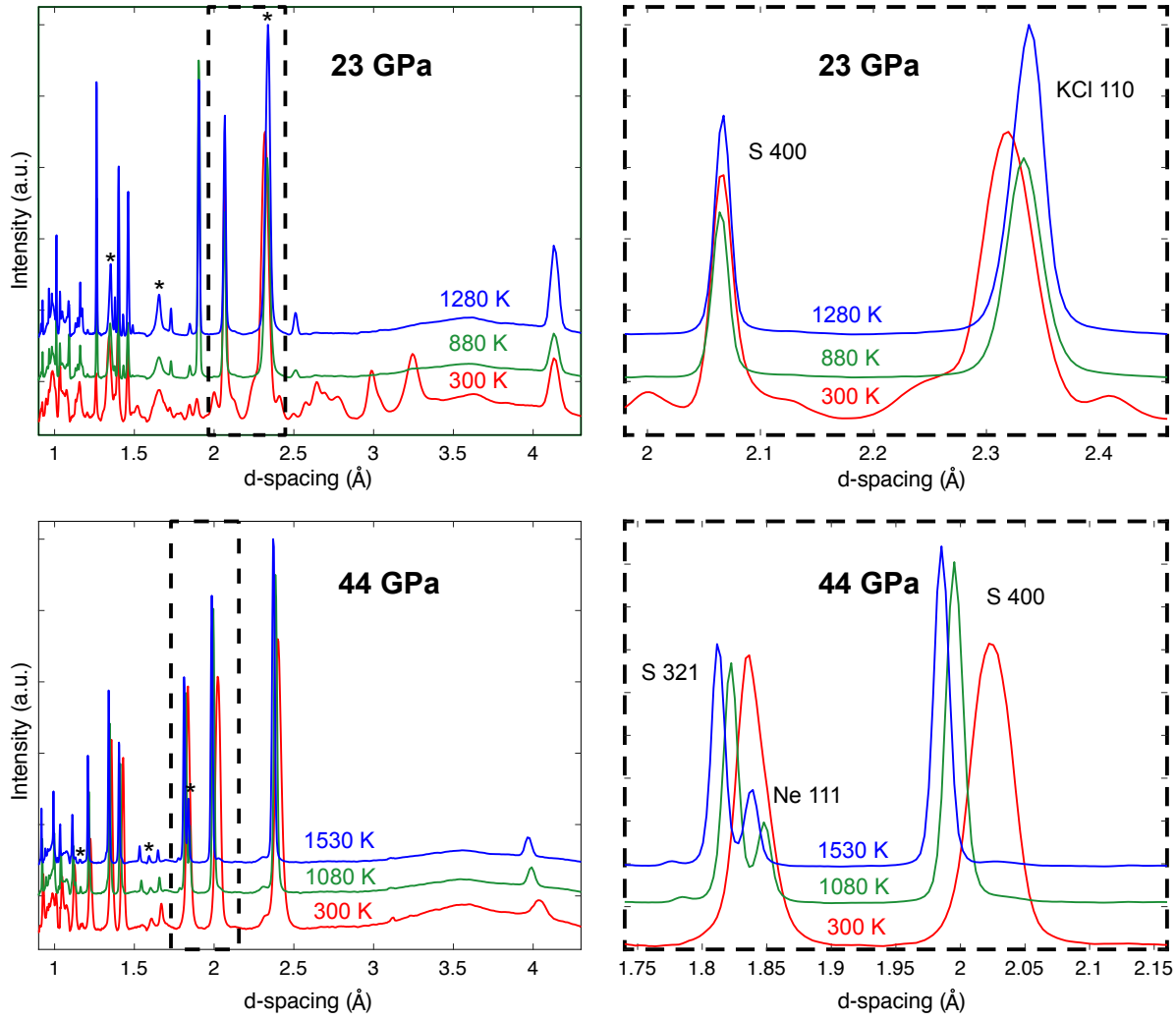

FIG. 7. Selected heating patterns of tetragonal sulfur using B2 KCl insulation (top panels) and solid Ne insulation (bottom panels). The right panels show a zoom-in of the dashed regions with insulation and sulfur peaks. Volumes of these patterns from fitting 8 – 10 peaks for sulfur and 3 peaks for KCl/Ne are shown in Table S2. A discussion of the pressure change may be found in the Supplementary Materials.

IV. DISCUSSION AND CONCLUSION

Our measured kink-free melting curve of sulfur in the range of 26 – 65 GPa is consistent with an absence of solid phase transitions in this region and is supported by our in-situ x-ray diffraction measurements of tetragonal sulfur below the melting curve. The Clapeyron slope of the melting curve is ∼14 K/GPa and decreases with increasing pressure as the melting

curve flattens. Some of our quenched samples show anomalous thin, elongated fiber-like textures which may correlate to quenching of fibrous sulfur[39]. Other quenched samples show holes where molten sulfur rose up into the insulation medium (Fig. 2). These quenched textures in conjunction with other diagnostics may help quantify the viscosity of sulfur at high pressures and hence may be used to study anomalous liquid structure and liquid-liquid phase transitions[2,40] when combined with a full set of time-resolved experiments.

Melting curve maxima have been commonly observed for many pure elements, including other group VI elements like Te at 1.2 GPa[16]and Se at 10 GPa[41] as well as P at 1 GPa[42] and N at 50-70 GPa[43–45] to name a few. Previous studies suggested that the melting curve of sulfur have local maxima at 1.7 GPa[18] and 8 GPa[2]. It was hypothesized that the liquid-liquid phase transition at 12 GPa would cause another local maximum in the melting curve[3]. If that is indeed the case, the melting curve of sulfur would have to change concavity again between 12 – 23 GPa in order to be commensurate with the shape of our melting curve above 23 GPa.

According to our in-situ diffraction, the stability range of tetragonal sulfur is likely to extend to 65 GPa, the highest pressure of melting temperature measured in this study, at high temperatures up to the melting point. The nature of the orthorhombic *Fddd*-to-trigonal transition is still not well defined. One study finds a nearly constant transition temperature of 580 ± 20 K from between 2 GPa and 11 GPa[38], while another finds the transition occurring near the melting curve or just above room temperature (Fig. 8)[13]. Pyrometric temperature measurement in the LHDAC has limited temperature resolution below 1000 K because we use visible wavelengths most sensitive to the 600 nm – 900 nm range, so further experiments using external resistance heating in the range of 10 – 20 GPa will help define the tetragonal sulfur stability range and the phase boundary between orthorhombic *Fddd*-to-trigonal transition.

This study demonstrates the first LHDAC study of sulfur, showing that its high-temperature solid phases and melting can be successfully probed using the four-color temperature measurement and mapping technique[21,28]. Characterizing the shape of the melting curve and the structure of liquid sulfur at high pressures will allow us to better understand the role of sulfur as an endmember in complex systems such as Fe-S-O and Fe-S-Si, which show immiscibility persisting at high pressures[46,47] and are commonly invoked materials for planetary cores. Sulfur's low melting temperature which persists to 65 GPa

distinguishes it from common silicates and oxides. Such a low melting temperature would drastically change rheological properties and provide a metric for identifying planets with significant sulfur in their interiors.

---

[1] I. R. Kaplan and J. R. Hulston, Geochimica et Cosmochimica Acta **30**, 479 (1966).

[2] V. Brazhkin, R. Voloshin, S. Popova, and A. Umnov, Physics Letters A **154**, 413 (1991).

[3] V. Brazhkin, S. Popova, and R. Voloshin, Physica B: Condensed Matter **265**, 64 (1999).

[4] H. Luo and A. L. Ruoff, Physical Review B **48**, 569 (1993).

[5] Y. Akahama, M. Kobayashi, and H. Kawamura, Physical Review B **48**, 6862 (1993).

[6] H. Luo, R. G. Greene, and A. L. Ruoff, Physical Review Letters **71**, 2943 (1993).

[7] C. Hejny, L. Lundegaard, S. Falconi, M. McMahon, and M. Hanfland, Physical Review B **71**, 020101 (2005).

[8] O. Degtyareva, E. Gregoryanz, H. Mao, and R. Hemley, High Pressure Research **25**, 17 (2005).

[9] L. Crapanzano, W. A. Crichton, G. Monaco, R. Bellissent, and M. Mezouar, Nature Materials **4**, 550 (2005).

[10] R. Steudel and B. Eckert, in *Elemental sulfur and sulfur-rich compounds I* (Springer, 2003) pp. 1–80.

[11] T. Fujimori, A. Morelos-Gómez, Z. Zhu, H. Muramatsu, R. Futamura, K. Urita, M. Terrones, T. Hayashi, M. Endo, S. Y. Hong, *et al.*, Nature communications **4**, 2162 (2013).

[12] H. Fujihisa, Y. Akahama, H. Kawamura, H. Yamawaki, M. Sakashita, T. Yamada, K. Honda, and T. Le Bihan, Physical Review B **70**, 134106 (2004).

[13] O. Degtyareva, E. Gregoryanz, M. Somayazulu, P. Dera, H.-k. Mao, and R. J. Hemley, Nature materials **4**, 152 (2005).

[14] B. Meyer, T. Oommen, and D. Jensen, The Journal of Physical Chemistry **75**, 912 (1971).

[15] L. Liu, Y. Kono, C. Kenney-Benson, W. Yang, Y. Bi, and G. Shen, Physical Review B **89**, 174201 (2014).

[16] B. Deaton and F. Blum Jr, Physical Review **137**, A1131 (1965).

[17] K. Ward Jr and B. Deaton, Physical Review **153**, 947 (1967).

[18] G. C. Vezzoli, F. Dachille, and R. Roy, Inorganic Chemistry **8**, 2658 (1969).

[19] H. Luo, S. Desgreniers, Y. K. Vohra, and A. L. Ruoff, Physical Review Letters **67**, 2998 (1991).

[20] Y. Meng, R. Hrubiak, E. Rod, R. Boehler, and G. Shen, Review of Scientific Instruments **86**, 072201 (2015).

[21] Z. Du, G. Amulele, L. R. Benedetti, and K. K. M. Lee, Review of Scientific Instruments **84**, 075111 (2013).

[22] J. Deng, Z. Du, R. Bendetti, and K. K. M. Lee, Journal of Applied Physics **121**, 025901 (2017).

[23] Z. Du, T. Gu, V. Dobrosavljevic, S. T. Weir, S. Falabella, and K. K. M. Lee, Review of Scientific Instruments **86**, 095103 (2015).

[24] S. Rettig and J. Trotter, Acta Crystallographica Section C: Crystal Structure Communications **43**, 2260 (1987).

[25] Y. Akahama and H. Kawamura, Journal of Applied Physics **96**, 3748 (2004).

[26] A. Dewaele, A. B. Belonoshko, G. Gabarino, F. Occelli, B. P., M. Hanfland, and M. Mezouar, Physical Review B **85**, 214105 (2012).

[27] Y. Fei, A. Ricolleau, M. Frank, K. Mibe, G. Shen, and V. Prakapenka, Proceedings of the National Academy of Sciences **104**, 9182 (2007).

[28] Z. Du and K. K. M. Lee, Geophysical Research Letters **41**, 8061 (2014).

[29] K. Bröllos and G. Schneider, Berichte der Bunsengesellschaft für physikalische Chemie **78**, 296 (1974).

[30] M. Peanasky, C. Jurgensen, and H. Drickamer, Journal of Chemical Physics **81**, 6407 (1984).

[31] L. Yang, A. Karandikar, and R. Boehler, Review of Scientific Instruments **83**, 063905 (2012).

[32] K. Hirose, G. Morard, K. Umemoto, J. Hernlund, G. Helffrich, and S. Labrosse, Nature **543**, 99 (2017).

[33] S. Deemyad, E. Sterer, C. Barthel, S. Rekhi, J. Tempere, and I. F. Silvera, Review of scientific instruments **76**, 125104 (2005).

[34] S. Anzellini, A. Dewaele, M. Mezouar, P. Loubeyre, and G. Morard, Science **340**, 464 (2013).

[35] A. Lazicki, Y. Fei, and R. J. Hemley, Solid State Communications **150**, 625 (2010).

[36] Z. M. Geballe and R. Jeanloz, American Mineralogist **99**, 720 (2014).

[37] T. Bååk, Science **148**, 1220 (1965).

[38] L. Crapanzano, *Polymorphism of sulfur: structural and dynamical aspects*, Ph.D. thesis, Université Joseph-Fourier-Grenoble I (2006).

[39] M. Lind and S. Geller, The Journal of Chemical Physics **51**, 348 (1969).

[40] R. F. Bacon and R. Fanelli, Journal of the American Chemical Society **65**, 639 (1943).

[41] K. Tsuji, O. Shimomura, K. Tamura, and H. Endo, Zeitschrift für Physikalische Chemie **156**, 495 (1988).

[42] Y. Katayama, T. Mizutani, W. Utsumi, O. Shimomura, M. Yamakata, and K.-i. Funakoshi, Nature **403**, 170 (2000).

[43] G. D. Mukherjee and R. Boehler, Physical review letters **99**, 225701 (2007).

[44] A. F. Goncharov, J. C. Crowhurst, V. V. Struzhkin, and R. J. Hemley, Physical review letters **101**, 095502 (2008).

[45] D. Tomasino, Z. Jenei, W. Evans, and C.-S. Yoo, The Journal of chemical physics **140**, 244510 (2014).

[46] K. Tsuno, E. Ohtani, and H. Terasaki, Physics of the Earth and Planetary Interiors **160**, 75 (2007).

[47] C. Sanloup and Y. Fei, Physics of the Earth and Planetary Interiors **147**, 57 (2004).

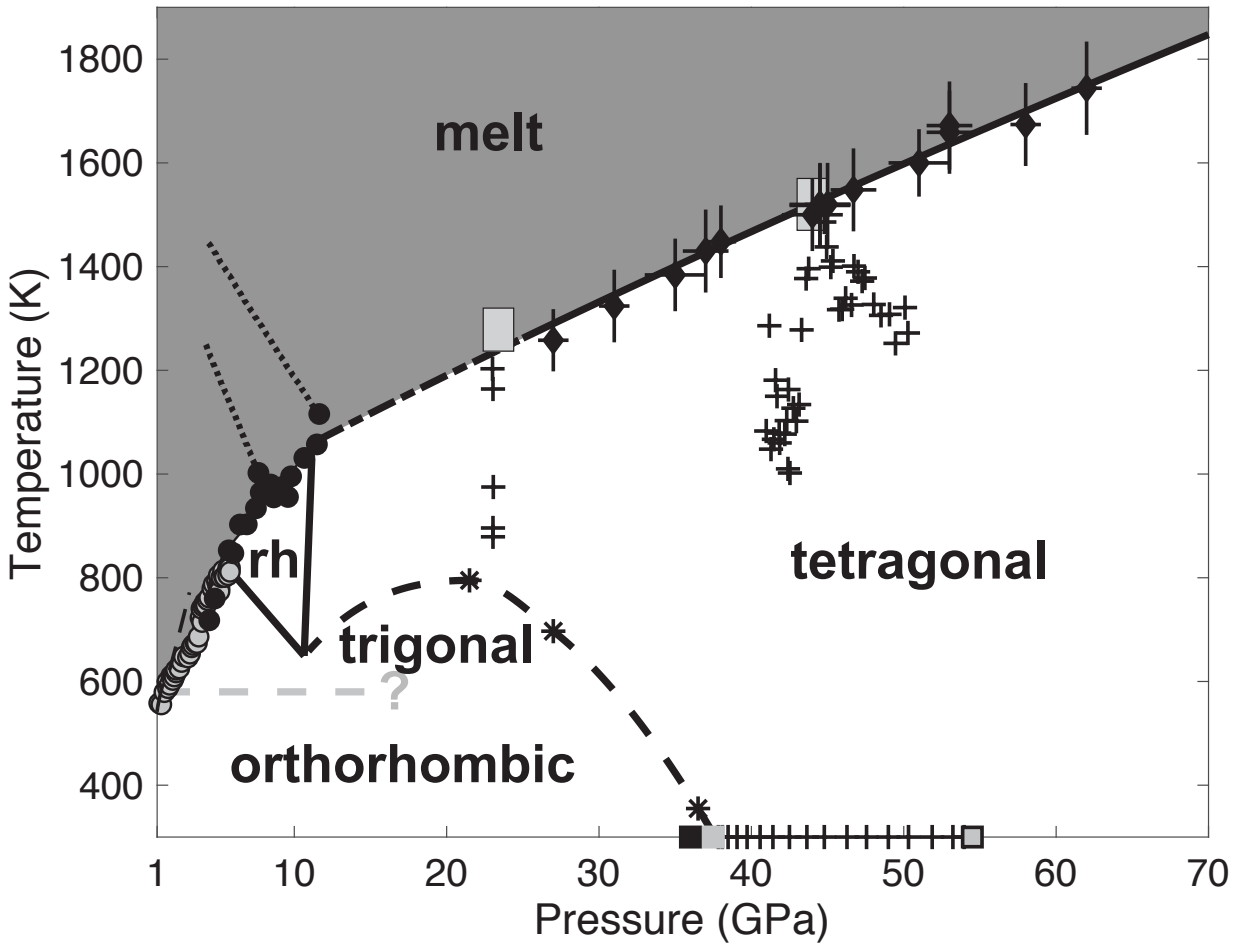

FIG. 8. The P,T diagram of sulfur to 70 GPa. Phases reported below 1 GPa (e.g., monoclinic) are not displayed due to a comparatively small stability field. The melt boundary above 26 GPa (black solid line) and the plus symbols indicating the tetragonal form of sulfur are from this study. Other melting data points and curves are from Ref.[16] (grey circles), Ref.[17] (thin dashed line), and Ref.[2] (black circles). The liquid-liquid transitions L-L' and L'-L" are from Ref.[2,3]. The trigonal-rhombohedral ("rh") and rhombohedral-tetragonal boundaries are from Ref.[9], the orthorhombic-trigonal transition boundary (grey dashed line) is from Ref.[38], and the trigonal-tetragonal boundary (thick dashed line) is inferred from Ref.[9,13]. The asterisks on the trigonal-tetragonal boundary are discrete transition points from Ref.[13]. Solid phase boundaries that are shown in dashed lines are speculative due to few points or discrepancies between studies. The filled squares at room temperature represent reported transition to tetragonal sulfur from this study (plus symbol), Ref.[8] (black), Ref.[7] (grey), and Ref.[5] (grey with black outline).